
Riemannian Manifold Kernel for Persistence Diagrams

Tam Le¹ Makoto Yamada¹

Abstract

Algebraic topology methods have recently played an important role for statistical analysis with complicated geometric structured data. Among them, *persistent homology* is a well-known tool to extract robust topological features, and outputs as *persistence diagrams*. Unfortunately, persistence diagrams are point multi-sets which can not be used in machine learning algorithms for vector data. To deal with it, an emerged approach is to use kernel methods. Besides that, geometry for persistence diagrams is also an important factor. A popular geometry for persistence diagrams is the *Wasserstein metric*. However, Wasserstein distance is not *negative definite*. Thus, it is limited to build positive definite kernels upon the Wasserstein distance *without approximation*. In this work, we explore an alternative *Riemannian manifold geometry*, namely the Fisher information metric. By building upon the *geodesic* distance on the Riemannian manifold, we propose a positive definite kernel, namely Riemannian manifold kernel. Then, we analyze eigensystem of the integral operator induced by the proposed kernel for kernel machines. Based on that, we conduct generalization error bounds via covering numbers and Rademacher averages for kernel machines using the Riemannian manifold kernel. Additionally, we also show some nice properties for the proposed kernel such as stability, infinite divisibility and comparative time complexity with other kernels for persistence diagrams in term of computation. Throughout experiments with many different tasks on various benchmark datasets, we illustrate that the Riemannian manifold kernel improves performances of other baseline kernels.

1. Introduction

Using algebraic topology methods for statistical data analysis has been recently received a lot of attention from machine learning community (Chazal et al., 2015; Kwitt et al., 2015; Bubenik, 2015; Kusano et al., 2016; Chen and Quadrianto, 2016; Carriere et al., 2017; Hofer et al., 2017; Adams et al., 2017; Kusano et al., to appear in 2018). 0-dimensional topological features, which are connected components of data, are analogous to clustering methods in machine learning. Moreover, high dimensional topological features represent higher level information such as rings, cavities corresponding for 1-dimensional and 2-dimensional topological features respectively, which can be useful to deal with complicated geometric structured data. For examples, algebraic topology methods are applied in various research fields such as biology (Kasson et al., 2007; Xia and Wei, 2014; Cang et al., 2015), brain science (Singh et al., 2008; Lee et al., 2011; Petri et al., 2014), and information science (De Silva et al., 2007; Carlsson et al., 2008).

In algebraic topology, *persistent homology* is an important method to extract robust topological information, it outputs point multisets, called *persistence diagrams* (PDs) (Edelsbrunner et al., 2000). PDs can have various sizes. Therefore, we can not directly plug PDs into traditional statistical machine learning algorithms, which often assume a vector representation for data. One of prominent approaches is to use kernel methods for PDs (Reininghaus et al., 2015; Kusano et al., 2016; Carriere et al., 2017). Moreover, geometry on PDs also plays an important role. One of the most popular geometries for PDs is the Wasserstein metric (Villani, 2003; Peyre and Cuturi, 2017). However, it is well-known that the Wasserstein distance is not *negative definite* (Reininghaus et al., 2015) (Appendix A). Consequently, we may not obtain positive definite kernels, built upon from the Wasserstein distance. It may be necessary to *approximate* the Wasserstein distance to achieve positive definiteness for kernels, relied on Wasserstein geometry. For example, (Carriere et al., 2017) used the sliced Wasserstein (SW) distance—an *approximation* of Wasserstein distance—to construct the positive definite SW kernel.

In this work, we explore an alternative Riemannian manifold geometry, namely the Fisher information metric (Amari and Nagaoka, 2007; Lee, 2006). Based on the geodesic distance

¹RIKEN, Japan. Correspondence to: Tam Le <tam.le@riken.jp>.

between PDs in the Riemannian manifold, we proposed a positive definite kernel, namely Riemannian manifold kernel. The proposed kernel well preserves the geometry of the Riemannian manifold since it is directly built upon the *geodesic distance without approximation*. We then derive the eigensystem of the integral operator induced by the Riemannian manifold kernel for kernel machines. Based on that, we derive generalization error bounds via covering numbers and Rademacher averages for kernel machines using the proposed kernel. Furthermore, we also provide some nice properties for the proposed kernel such as (i) a bound for the proposed kernel induced squared distance with respect to the geodesic distance which can be interpreted as stability in a similar sense as the work of (Kwitt et al., 2015; Reininghaus et al., 2015) with Wasserstein geometry, (ii) infinite divisibility for the proposed kernel, and (iii) comparative time complexity with other kernels for PDs on computation.

The paper is organized as follows: we give a preliminary about PDs with the Wasserstein geometry and the Riemannian manifold geometry, as well as some important theorems about kernels in Section 2. In Section 3, we describe the proposed Riemannian manifold kernel and prove that it is positive definite. Then, we provide theoretical analysis about the eigensystem of the integral operator induced with our proposed kernel, and generalization error bounds on covering numbers and Rademacher averages, as well as bounds on the proposed kernel induced squared distance with respect to the geodesic distance of the Riemannian manifold between PDs and infinite divisibility of our proposed kernel in Section 4. After that, we review related work in Section 5. We then illustrate that our proposed kernel improves performances of other baseline kernels through experiments with many different learning tasks on various benchmark datasets in Section 6. Finally, we conclude it in Section 7.

2. Preliminary

2.1. Persistence Diagrams with Wasserstein Metric

Persistence diagrams. Given a data set X , we transform X into a filtration $\mathbb{F}(X)$, defined as $\mathbb{F} = \{F_a \mid a \in \mathbb{R}\}$ ¹, then compute its persistent homology $H(\mathbb{F}(X))$ to obtain persistence diagrams $Dg(\mathbb{F}(X))$ as a 2-dimensional point multiset². Each point $(u, v) \in \mathbb{R}^2$ in the persistence diagrams represents a lifespan of a particular topological feature such as a connected component, a ring, or a cavity, having a birth at F_u , and a death at F_v . For more details about mathematical definitions of persistence diagrams, we refer to (Chazal and Michel, 2017; Kusano et al., to appear in 2018). We then provide some popular filtrations to

¹For $a \leq b$, F_a is a sub-complex of F_b .

²A point multiset is a set with multiplicity of each point.

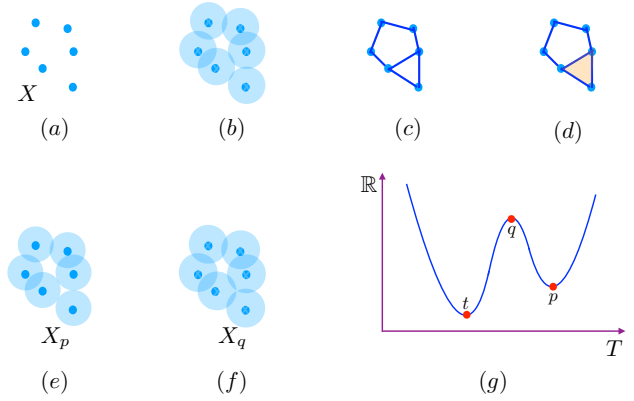


Figure 1. An illustration for persistence diagrams with some popular filtrations. (a) A set of points as an input. (b) A ball model filtration. (c) Čech complex filtration. (d) Vietoris-Rips complex filtration (it has only 1 ring since it contains a 2-simplex, illustrated as the orange triangle). (e) An illustration of a birth for a ring in the ball model filtration. (f) An illustration of a death for a ring in the ball model filtration. (g) A sub-level set filtration (a connected component has a birth at X_p , and a death at X_q). In this illustration, both the ball model filtration and Čech complex filtration have 2 rings, but there is only 1 ring for Vietoris-Rips complex filtration due to the 2-simplex. For sub-level set filtration, there are 2 connected components (p, q) and (t, ∞) . Hence, the persistence diagram of 0-dimension topological feature is that $Dg = \{(p, q); (t, \infty)\}$.

illustrate persistence diagrams as follows,

(i) Ball model filtration. Let $X = \{x_1, x_2, \dots, x_m\}$ be a finite set in a metric space as in Figure 1 (a), and $B(x, a)$ be a ball with a center x and a radius a . We denote $X_a := \cup_{x_i \in X} B(x_i, a)$ for $a \geq 0$. For $a < 0$, we define $X_a := \emptyset$. Therefore, $\{X_a \mid a \in \mathbb{R}\}$ can be used as a filtration, illustrated in Figure 1 (b). For example, Figure 1 (e) shows a birth for a ring at X_p while Figure 1 (f) illustrates that the ring is death at X_q . Therefore, a point (p, q) is in the persistence diagram of 1-dimensional topological feature for the set X .

(ii) Čech complex filtration. Given a set $X = \{x_1, x_2, \dots, x_m\}$ in a metric space (T, d_T) . For $a \geq 0$, we form a t -simplex from a $(t+1)$ -point subset X_{t+1} of X if there exist $x' \in M$, such that $d_T(x, x') \leq a, \forall x \in X_{t+1}$. The set of all these simplices is called the Čech complex of X with parameter $a \geq 0$, denoted as $\mathfrak{C}(X, a)$. For $a < 0$, we define $\mathfrak{C}(X, a) := \emptyset$. Therefore, $\{\mathfrak{C}(X, a) \mid a \in \mathbb{R}\}$ can be considered as a filtration and illustrated in Figure 1 (c). When $T \subset \mathbb{R}^q$, the topology of $\mathfrak{C}(X, a)$ is homotopy equivalent to X_a (Hatcher, 2002) (p. 257). Consequently, the persistence diagrams with Čech complex filtration equals

to the persistence diagrams with ball model filtration.

(iii) Vietoris-Rips complex (a.k.a. Rips complex) filtration. Given a set $X = \{x_1, x_2, \dots, x_m\}$ in a metric space (T, d_T) . For $a \geq 0$, we form a t -simplex from a $(t+1)$ -point subset X_{t+1} of X which satisfies $d_T(x, z) \leq 2a, \forall x, z \in X_{t+1}$. The set of all these simplices is called Vietoris-Rips complex of X with parameter $a \geq 0$, denoted as $\mathfrak{R}(X, a)$. For $a < 0$, we define $\mathfrak{R}(X, a) = \emptyset$. Therefore, $\{\mathfrak{R}(X, a) \mid a \in \mathbb{R}\}$ can be used as a filtration as illustrated in Figure 1 (d).

(iv) Sub-level set filtration. Let T be a topological space, given a function $f : T \rightarrow \mathbb{R}$ as an input, and defined a sub-level set $\mathfrak{F}_a := f^{-1}((-\infty, a])$. Thus, $\{\mathfrak{F}_a \mid a \in \mathbb{R}\}$ can be regarded as a filtration as in Figure 1 (g). For example, it is easy to see that a connected component has a birth at \mathfrak{F}_p and it is death at \mathfrak{F}_q as in Figure 1 (g). Thus, a point (p, q) is in persistence diagrams of 0-dimensional topological feature for the given function f . In Figure 1 (g), persistence diagram of 0-dimensional topological feature for f is $Dg = \{(p, q); (t, \infty)\}$.

Wasserstein metric for persistence diagrams. Persistence diagram Dg can be considered as a discrete measure $\mu_{Dg} = \sum_{p \in Dg} \delta_p$ where δ_p is the Dirac unit mass on p . Therefore, the ∞ -Wasserstein metric (a.k.a bottleneck) is a popular choice to measure distances on the set \mathbb{D} of persistence diagrams with bounded cardinalities. Given two persistence diagrams Dg_i and Dg_j , the ∞ -Wasserstein distance \mathcal{W}_∞ (Cohen-Steiner et al., 2007; Carriere et al., 2017; Adams et al., 2017) is defined as

$$\mathcal{W}_\infty(Dg_i, Dg_j) = \inf_{\gamma} \sup_{p \in Dg_i \cup \Delta} \|p - \gamma(p)\|_\infty, \quad (1)$$

where $\Delta := \{(a, a) \mid a \in \mathbb{R}\}$ is the diagonal set, and $\gamma : Dg_i \cup \Delta \rightarrow Dg_j \cup \Delta$ is bijective. Moreover, $(\mathbb{D}, \mathcal{W}_\infty)$ is a metric space.

2.2. From Wasserstein Metric to Riemannian Metric

Wasserstein metric measures a distance between probability distributions³. However, Wasserstein distance is not *negative definite* (Reininghaus et al., 2015) (Appendix A). Therefore, it is limited to apply kernel methods based on Wasserstein geometry. For example, (Kolouri et al., 2016; Carriere et al., 2017) used an *approximation* of Wasserstein distance, namely sliced Wasserstein distance, to obtain positive definite kernels.

In this paper, we explore a particular Riemannian metric on the probability simplex \mathbb{P} , namely the Fisher information metric (FIM).

³Wasserstein distance is also applicable to a space of nonnegative, not necessarily normalized, measures with a same mass (Carriere et al., 2017).

FIM is the well-known geometry for probability distributions, especially in information geometry (Amari and Nagaoka, 2007). FIM can be also regarded as a pull-back metric from the Euclidean metric on the positive orthant of the sphere \mathbb{S}^+ . Indeed, let us define a diffeomorphism mapping $h : \mathbb{P} \rightarrow \mathbb{S}^+$ as the Hellinger mapping $h(x) := \sqrt{x}$, where the square root is an element-wise function. The mapping h pulls-back the Euclidean metric \mathcal{S} on the positive orthant of the sphere \mathbb{S}^+ to the Fisher information metric \mathcal{P} on the probability simplex \mathbb{P} . Let u, v be tangent vectors in the tangent space $T_x \mathbb{P}$ on the probability simplex \mathbb{P} at a point $x \in \mathbb{P}$, so we have

$$\mathcal{P}_x(u, v) := h^* \mathcal{S}_x(u, v) = \mathcal{S}_{h(x)}(h_* u, h_* v), \quad (2)$$

where $h^* \mathcal{S}$ is a pull-back metric on the probability simplex \mathbb{P} from the Euclidean metric \mathcal{S} on the positive orthant of the sphere \mathbb{S}^+ through the diffeomorphism Hellinger mapping h , and h_* is the push-forward operator which maps a tangent vector $u \in T_x \mathbb{P}$ to a tangent vector $h_* u \in T_{h(x)} \mathbb{S}^+$. Therefore, the Hellinger mapping h is an isometric mapping between the probability simplex \mathbb{P} and the positive orthant of the sphere \mathbb{S}^+ . Consequently, the *geodesic* distance between two probability distributions x and z under the Fisher information metric \mathcal{P} —a Riemannian metric—on the probability simplex \mathbb{P} is equivalent to the length of the shortest curve on the positive orthant of the sphere \mathbb{S}^+ between two corresponding mapped points $h(x)$ and $h(z)$. So, we have

$$d_{\mathcal{P}}(x, z) = \arccos(\langle h(x), h(z) \rangle), \quad (3)$$

where $\langle \cdot, \cdot \rangle$ is the Euclidean inner product.

2.3. Kernels

Positive definite kernels. A function $k : X \times X \rightarrow \mathbb{R}$ is called a positive definite kernel if $\forall n \in \mathbb{N}^*, \forall x_1, x_2, \dots, x_n \in X, \sum_{i,j} c_i c_j k(x_i, x_j) \geq 0, \forall c_i \in \mathbb{R}$.

Negative definite kernels. A function $k : X \times X \rightarrow \mathbb{R}$ is called a negative definite kernel if $\forall n \in \mathbb{N}^*, \forall x_1, x_2, \dots, x_n \in X, \sum_{i,j} c_i c_j k(x_i, x_j) \leq 0, \forall c_i \in \mathbb{R}$ such that $\sum_i c_i = 0$.

Berg-Christensen-Ressel Theorem. In (Berg et al., 1984) (Theorem 3.2.2, p.74), if κ is a *negative definite* kernel, then $k_t(x, z) := \exp(-t\kappa(x, z))$ is a positive definite kernel for all $t > 0$. For example, Gaussian kernel $k_t(x, z) = \exp(-t \|x - z\|_2^2)$ is positive definite since it is easy to check that squared Euclidean distance is indeed a negative definite kernel⁴.

⁴ $\forall n \in \mathbb{N}^*, \forall x_1, x_2, \dots, x_n \in X$, and $\forall c_i \in \mathbb{R}$ such that $\sum_i c_i = 0$, we have $\sum_{i,j} c_i c_j \|x_i - x_j\|_2^2 = \sum_i c_i x_i^2 \sum_j c_j + \sum_i c_i \sum_j c_j x_j^2 - 2 \sum_{i,j} c_i c_j x_i x_j = -2 (\sum_i c_i x_i)^2 \leq 0$.

Schoenberg Theorem. In (Schoenberg, 1942) (Theorem 2, p. 102), a function $f(\langle \cdot, \cdot \rangle)$ defined on the unit sphere in a Hilbert space is positive definite if and only if its Taylor series expansion has only nonnegative coefficients,

$$f(\xi) = \sum_{i=0}^{\infty} a_i \xi^i, \quad \text{with } a_i \geq 0. \quad (4)$$

3. The Riemannian Manifold Kernel for Persistence Diagrams is Positive Definite

For the ∞ -Wasserstein distance \mathcal{W} in Equation (1), two persistent diagrams Dg_i and Dg_j may be two discrete measures with different masses. So, the transportation plan γ is bijective between $Dg_i \cup \Delta$ and $Dg_j \cup \Delta$ instead of between two discrete measures Dg_i and Dg_j . (Carriere et al., 2017), for instance, used Wasserstein distance between two persistent diagrams Dg_i and Dg_j where its transportation plans operate between $Dg_i \cup Dg_{j\Delta}$ and $Dg_j \cup Dg_{i\Delta}$ (non-negative, not necessarily normalized measures with same masses). Here, we denote $Dg_{i\Delta} := \{\Pi_{\Delta}(p) \mid p \in Dg_i\}$ where $\Pi_{\Delta}(p)$ is a projection of a point p on the diagonal set Δ . Following this line of work, we also consider a distance between two measures $Dg_i \cup Dg_{j\Delta}$ and $Dg_j \cup Dg_{i\Delta}$ as a distance between two persistent diagrams Dg_i and Dg_j . To this end, we first introduce a probabilistic representation for a discrete measure via normalization and smoothness, before giving the definition of the Riemannian metric for PDs.

Normalization and smoothness for discrete measures.

Given a discrete measure $\mu_{\Omega} = \sum_{p \in \Omega} \delta_p$, and a bandwidth $\sigma > 0$, we propose to smooth and normalize μ_{Ω} as a probability distribution ρ_{Ω} , written as follows

$$\rho_{\Omega} := \frac{1}{Z} \sum_{p \in \Omega} \mathbb{N}(p, \sigma I), \quad (5)$$

where \mathbb{N} is a Gaussian function, I is an identity matrix, and Z is a partition function for normalization (i.e. $Z = \int \sum_{p \in \Omega} \mathbb{N}(x; p, \sigma I) dx$). When we have a priori knowledge about a degree of importance for a mean p , we can extend Equation (5) by some weight scheme for its corresponding Gaussian function $\mathbb{N}(p, \sigma I)$. Additionally, when $\sigma \rightarrow 0$, then $\mathbb{N}(p, \sigma I) \rightarrow \delta_p$, and ρ turns into a normalization for discrete measures without smoothing.

Definition 1. Let Dg_i, Dg_j be two finite and bounded persistence diagrams. The Riemannian metric between Dg_i and Dg_j is defined as follows,

$$d_{RM}(Dg_i, Dg_j) := d_{\mathcal{P}} \left(\rho_{(Dg_i \cup Dg_{j\Delta})}, \rho_{(Dg_j \cup Dg_{i\Delta})} \right). \quad (6)$$

Lemma 3.1. Let X be the set of bounded and finite persistent diagrams. Then, $(d_{RM} - \tau)$ is negative definite on X for all $\tau \geq \frac{\pi}{2}$.

Proof. Let consider the function $\tau - \arccos(\xi)$ where $\tau \geq \frac{\pi}{2}$ and $\xi \in [0, 1]$, then apply the Taylor series expansion for $\arccos(\xi)$ at 0, we have

$$\tau - \arccos(\xi) = \tau - \frac{\pi}{2} + \sum_{i=0}^{\infty} \frac{(2i)!}{2^{2i}(i!)^2(2i+1)} x^{2i+1}. \quad (7)$$

So, all coefficients of the Taylor series expansion are non-negative. Following the Schoenberg Theorem (in Section 2.3), for $\tau \geq \frac{\pi}{2}$ and $\xi \in [0, 1]$, $\tau - \arccos(\xi)$ is positive definite. Consequently, $\arccos(\xi) - \tau$ is negative definite.

Furthermore, X is the set of bounded and finite persistent diagrams, from Equation (6) and Equation (3), the range of the Euclidean inner product is $[0, 1]$ since the Hellinger mapping h of a smoothed and normalized measure $\rho_{(\cdot)}$ is on the positive orthant of the sphere \mathbb{S}^+ .

Hence, $d_{RM} - \tau$ is negative definite on X for all $\tau \geq \frac{\pi}{2}$. ■

Lemma 3.2. Let X be the set of bounded and finite persistent diagrams. Then, $\forall n \in \mathbb{N}^*, \forall x_1, x_2, \dots, x_n \in X$ and $\forall t > 0$, the Riemannian manifold kernel,

$$k_{RM}(x_i, x_j) := \exp(-td_{RM}(x_i, x_j)), \quad (8)$$

is positive definite on X .

Proof. We rewrite the kernel as follows

$$k_{RM}(x_i, x_j) = \alpha \exp(-t(d_{RM}(x_i, x_j) - \tau)), \quad (9)$$

where $\alpha = \exp(-t\tau)$. Let choose $\tau \geq \frac{\pi}{2}$, then apply Lemma 3.1, and the Berg-Christensen-Ressel Theorem (in Section 2.3), we achieve that the proposed Riemannian manifold kernel k_{RM} is positive definite. ■

From Lemma 3.2, the Riemannian manifold kernel k_{RM} (Equation (8)) is directly built upon the Riemannian metric for PDs *without approximation*. Moreover, the proposed kernel is also positive definite.

Computation. Given two finite PDs Dg_i and Dg_j with cardinalities bounded by $N \in \mathbb{N}^*$, in practice, we consider a set $\Theta := Dg_i \cup Dg_{j\Delta} \cup Dg_j \cup Dg_{i\Delta}$ without multiplicity in \mathbb{R}^2 for smoothed and normalized measures $\rho_{(\cdot)}$. Then, let m be the cardinality of Θ , we have $m \leq 4N$. Consequently, the time complexity of the normalization and smoothness for discrete measures is $O(Nm)$. Especially, we can reduce this time complexity into $O(N + m)$ by approximation with bounded error using the Fast Gauss Transform (Greengard and Strain, 1991; Morariu et al., 2009). Additionally, $d_{\mathcal{P}}$ (Equation (3)) is evaluated between two points in the m -dimensional probability simplex \mathbb{P}_{m-1} . So, the time complexity of the Riemannian manifold kernel k_{RM} between two smoothed and normalized measures is

$O(m)$. Hence, the time complexity of k_{RM} between Dg_i and Dg_j is $O(N^2)$, or $O(N)$ for the approximation with a bounded error using Fast Gauss Transform. We recall that the time complexity of the Wasserstein distance between Dg_i and Dg_j is $O(N^3 \log(N))$ (Pele and Werman, 2009) (§2.1). For the Sliced Wasserstein distance which is an approximation of Wasserstein distance, the time complexity is $O(N^2 \log(N))$ (Carriere et al., 2017), or $O(MN \log(N))$ for its approximation with M projections (Carriere et al., 2017).

4. Theoretical Analysis

In this section, we analyze for the Riemannian manifold kernel k_{RM} (in Equation (8)) where the Hellinger mapping h of a smoothed and normalized measure $\rho(\cdot)$ is on the positive orthant of the d -dimension unit sphere in \mathbb{R}^d , defined as $\mathbb{S}_{d-1}^+ := \{x \mid x \in \mathbb{R}_+^d, \|x\|_2 = 1\}$. Let Dg_i, Dg_j be PDs in the set of bounded and finite persistent diagrams X . We denote x_i and $x_j \in \mathbb{S}_{d-1}^+$ as corresponding mapped points through the Hellinger mapping h of smoothed and normalized measures $\rho_{(Dg_i \cup Dg_j)^\Delta}$ and $\rho_{(Dg_j \cup Dg_i)^\Delta}$ respectively. Then, we rewrite the Riemannian manifold kernel between x_i and x_j as follows,

$$k_{RM}(x_i, x_j) = \exp(-t \arccos(\langle x_i, x_j \rangle)). \quad (10)$$

Eigensystem. Let $T_{k_{RM}} : L_2(\mathbb{S}_{d-1}^+, \mu) \rightarrow L_2(\mathbb{S}_{d-1}^+, \mu)$ be the integral operator induced by the Riemannian manifold kernel k_{RM} , which is defined as $(T_{k_{RM}}f)(x) := \int k_{RM}(x, y)f(y)d\mu(y)$, where $(\mathbb{S}_{d-1}^+, \mu)$ is a probability space. Following (Smola et al., 2001) (Lemma 4), we derive an eigensystem of the integral operator $T_{k_{RM}}$ as in Proposition 1.

Proposition 1. Let $\{a_i\}_{i \geq 0}$ be the coefficients of Legendre polynomial expansion of the Riemannian manifold kernel $k_{RM}(x, z)$ defined on $\mathbb{S}_{d-1}^+ \times \mathbb{S}_{d-1}^+$ as in Equation (10),

$$k_{RM}(x, z) = \sum_{i=0}^{\infty} a_i P_i^d(\langle x, z \rangle), \quad (11)$$

where P_i^d is the associated Legendre polynomial of degree i . Let $|\mathbb{S}_{d-1}| := \frac{2\pi^{d/2}}{\Gamma(d/2)}$ denote the surface of \mathbb{S}_{d-1} where $\Gamma(\cdot)$ is the Gamma function, $N(d, i) := \frac{(d+2i-2)(d+i-3)!}{(d-2)!i!}$ denote the multiplicity of spherical harmonics of order i on \mathbb{S}_{d-1} , and $\{Y_{i,j}^d\}_{1 \leq j \leq N(d,i)}$ denote any fixed orthonormal basis for the subspace of all homogeneous harmonics of order i on \mathbb{S}_{d-1} . Then, the eigensystem $(\lambda_{i,j}, \phi_{i,j})$ of the integral operator $T_{k_{RM}}$ induced by the Riemannian manifold kernel k_{RM} is as follows:

$$\phi_{i,j} = Y_{i,j}^d, \quad (12)$$

$$\lambda_{i,j} = \frac{a_i |\mathbb{S}_{d-1}|}{N(d, i)} \quad (13)$$

of multiplicity $N(d, i)$.

Proof. From the Addition Theorem (Muller, 2012) (Theorem 2, p. 18) and the Funk-Hecke formula (Muller, 2012) (§4, p. 29), we have

$$\sum_{j=1}^{N(d,i)} Y_{i,j}^d(x) Y_{i,j}^d(z) = \frac{N(d, i)}{|\mathbb{S}_{d-1}|} P_i^d(\langle x, z \rangle), \quad (14)$$

then replace P_i^d into Equation (11), and note that $\int_{\mathbb{S}_{d-1}} Y_{i,j}^d(x) Y_{i',j'}^d(x) dx = \delta_{i,i'} \delta_{j,j'}$, we complete the proof. \blacksquare

Corollary 4.0.1. All coefficients of Legendre polynomial expansion of the Riemannian manifold kernel are nonnegative.

Proof. From Lemma 3.1, the Riemannian manifold kernel k_{RM} is positive definite. Applying (Schoenberg, 1942) (Theorem 1, p. 101) for k_{RM} defined on $\mathbb{S}_{d-1}^+ \times \mathbb{S}_{d-1}^+$ as in Equation (10), we obtain the result. \blacksquare

The eigensystem of the integral operator $T_{k_{RM}}$ induced by the proposed kernel plays an important role to prove generalization error bounds for kernel machines using the proposed kernel via covering numbers and Rademacher averages as in Proposition 2 and Proposition 3 respectively.

Covering numbers. Given a set of finite points $S = \{x_i \mid x_i \in \mathbb{S}_{d-1}^+, d \geq 3\}$, the Riemannian manifold kernel hypothesis class with R -bounded weight vectors for S is defined as follows

$$\mathcal{F}_R(S) = \{f \mid f(x_i) = \langle w, \phi(x_i) \rangle_{\mathcal{H}}, \|w\|_{\mathcal{H}} \leq R\},$$

where $\langle \phi(x_i), \phi(x_j) \rangle_{\mathcal{H}} = k_{RM}(x_i, x_j)$. $\langle \cdot, \cdot \rangle_{\mathcal{H}}$ and $\|\cdot\|_{\mathcal{H}}$ are an inner product and a norm in the corresponding Hilbert space respectively. Following (Guo et al., 1999), we derive bounds on the generalization performance of the Riemannian manifold kernel on kernel machines via the covering numbers $\mathcal{N}(\cdot, \mathcal{F}_R(S))$ (Shalev-Shwartz and Ben-David, 2014) (Definition 27.1, p. 337) as in Proposition 2.

Proposition 2. Assume the number of non-zero coefficients $\{a_i\}$ in Equation (11) is finite, and r is the maximum index of the non-zero coefficients. Let $q := \arg \max_i \lambda_{i,i}$, choose $\alpha \in \mathbb{N}$ such that $\alpha < \left(\frac{\lambda_{q,q}}{\lambda_{i,i}}\right)^{\frac{N(d,q)}{2}}$ with $i \neq q$, and define $\varepsilon := 6R \sqrt{N(d, r) \left(a_q \alpha^{-2/N(d,q)} + \sum_{i=0, i \neq q}^{\infty} a_i\right)}$. Then, $\sup_{x_i \in S} \mathcal{N}(\varepsilon, \mathcal{F}_R(S)) \leq \alpha$.

Proof. From (Minh et al., 2006) (Lemma 3), we have $\|Y_{i,j}^d\|_{\infty} \leq \sqrt{\frac{N(d,i)}{|\mathbb{S}_{d-1}|}}$. It is easy to check that $\forall d \geq 3, i \geq$

$0, i \geq j$, we have $N(d, i) \geq N(d, j)$. Therefore, following Proposition 1, all eigenfunctions of k_{RM} satisfy that $Y_{i,j}^d \leq \sqrt{\frac{N(d,r)}{|\mathbb{S}_{d-1}|}}$. Additionally, the multiplicity of $\lambda_{i, \cdot}$ is $N(d, i)$, and $N(d, i)\lambda_{i, \cdot} = a_i |\mathbb{S}_{d-1}|$ (Equation (13)). Hence, from (Guo et al., 1999) (Theorem 1), we obtain the result. \blacksquare

Rademacher averages. We provide a different family of generalization error bounds via Rademacher averages (Bartlett et al., 2005). By plugging the eigensystem of the Riemannian manifold kernel as in Proposition 1 into the localized averages of function classes based on the Riemannian manifold kernel with respect to a fixed probability measure μ on \mathbb{S}_{d-1}^+ (Mendelson, 2003) (Theorem 2.1), we obtain a bound as in Proposition 3.

Proposition 3. Let $\{x_i\}_{1 \leq i \leq m}$ be independent, distributed according to μ on \mathbb{S}_{d-1}^+ , denote $\{\sigma_i\}_{1 \leq i \leq m}$ for independent Rademacher random variables, $\mathcal{H}_{k_{RM}}$ for the unit ball of the reproducing kernel Hilbert space corresponding with the Riemannian manifold kernel k_{RM} , and let $q := \arg \max_i \lambda_{i, \cdot}$. If $\lambda_{q, \cdot} \geq 1/m$, for $\tau \geq 1/(m|\mathbb{S}_{d-1}|)$, let

$$\Psi(\tau) := \sqrt{|\mathbb{S}_{d-1}|} \left(\sum_{a_i < \tau N(d, i)} a_i + \tau \sum_{a_i \geq \tau N(d, i)} N(d, i) \right),$$

then there are absolute constants C_ℓ and C_u which satisfy

$$C_\ell \Psi(\tau) \leq \mathbb{E} \sup_{\substack{\mathbf{f} \in \mathcal{H}_{k_{RM}} \\ \frac{\mathbb{E} \mu \mathbf{f}^2}{|\mathbb{S}_{d-1}|} \leq \tau}} \left| \sum_{i=1}^m \sigma_i \mathbf{f}(x_i) \right| \leq C_u \Psi(\tau), \quad (15)$$

where \mathbb{E} is an expectation.

From Proposition 2 and Proposition 3, a decay rate of the eigenvalues of the integral operator $T_{k_{RM}}$ is relative with the capacity of the kernel learning machines. When the decay rate of the eigenvalues is large, the capacity of kernel machines is reduced. So, if the training error of kernel machines is small, then it can lead to better bounds on generalization error.

Bounding for k_{RM} induced squared distance w.r.t. d_{RM} . The squared distance induced by the Riemannian manifold kernel, denoted as $d_{k_{RM}}^2$, can be computed by the Hilbert norm of the difference between two corresponding mappings. Given two persistent diagram Dg_i and Dg_j , we have $d_{k_{RM}}^2(Dg_i, Dg_j) := k_{RM}(Dg_i, Dg_i) + k_{RM}(Dg_j, Dg_j) - 2k_{RM}(Dg_i, Dg_j)$. We recall that k_{RM} is based on the Riemannian manifold geometry. So, it is of interest to bound the Riemannian manifold kernel induced squared distance $d_{k_{RM}}^2$ w.r.t. the corresponding geodesic distance d_{RM} of the Riemannian manifold between PDs as in Lemma 4.1.

Lemma 4.1. Let X be the set of bounded and finite persistent diagrams. Then, $\forall Dg_i, Dg_j \in X$, $d_{k_{RM}}^2(Dg_i, Dg_j) \leq$

$$2td_{RM}(Dg_i, Dg_j), \text{ where } t \text{ is a parameter of } k_{RM}.$$

Proof. We have

$$\begin{aligned} d_{k_{RM}}^2(Dg_i, Dg_j) &= 2(1 - k_{RM}(Dg_i, Dg_j)) \\ &= 2(1 - \exp(-td_{RM}(Dg_i, Dg_j))) \\ &\leq 2td_{RM}(Dg_i, Dg_j), \end{aligned}$$

$$\text{since } 1 - \exp(-u) \leq u, \forall u \geq 0. \quad \blacksquare$$

From Lemma 4.1, it implies that the Riemannian manifold kernel is stable on Riemannian manifold geometry in a similar sense as the work of (Kwitt et al., 2015; Reininghaus et al., 2015) on Wasserstein geometry.

Infinite divisibility for the Riemannian manifold kernel.

Lemma 4.2. The Riemannian manifold kernel k_{RM} is infinitely divisible.

Proof. For $m \in \mathbb{N}^*$, let $k_{RM_m} := \exp(-\frac{t}{m}d_{RM})$, so $(k_{RM_m})^m = k_{RM}$ and note that k_{RM_m} is positive definite. Hence, following (Berg et al., 1984) (§3, Definition 2.6), we have the result. \blacksquare

As for infinitely divisible kernels, the Gram matrix of the Riemannian manifold kernel does not need to be recomputed for each choice of t (Equation (8)), since it suffices to compute the Riemannian manifold distance between PDs in training set only once. This property is shared with the sliced Wasserstein kernel (Carriere et al., 2017). However, neither persistence scale space kernel (Reininghaus et al., 2015) nor persistence weighted Gaussian kernel (Kusano et al., 2016) has this property.

5. Related Work

Kernel methods for persistence diagrams (PDs) have been recently received much attention. For examples, (i) (Reininghaus et al., 2015) proposed the persistence scale space (PSS) kernel, motivated by a heat diffusion problem with a Dirichlet boundary condition. The PSS kernel between two PDs Dg_i and Dg_j is defined as $k_{PSS}(Dg_i, Dg_j) := \frac{1}{8\pi\sigma} \sum_{\substack{p_i \in Dg_i \\ p_j \in Dg_j}} \exp\left(-\frac{\|p_i - p_j\|_2^2}{8\sigma}\right) - \exp\left(-\frac{\|\bar{p}_i - \bar{p}_j\|_2^2}{8\sigma}\right)$, where σ is a scale parameter and if $p = (a, b)$, then $\bar{p} = (b, a)$, mirrored at the diagonal Δ . The time complexity is $O(N^2)$ where N is the bounded cardinality of PDs. By using the Fast Gauss Transform (Greengard and Strain, 1991) for approximation with bounded error, the time complexity can be reduced to $O(N)$. (ii) (Kusano et al., 2016) proposed the persistence weighted gaussian (PWG) kernel by using kernel embedding into the reproducing kernel Hilbert space.

Table 1. A comparison for time complexities and metric preservation of kernel methods for persistence diagrams where N is the bounded cardinality of persistence diagrams, and M is the number of projections to approximate the sliced Wasserstein distance. It is note that the sliced Wasserstein kernel is built upon the sliced Wasserstein distance which is an *approximation* of Wasserstein metric while the Riemannian manifold kernel uses the geodesic distance in Riemannian manifold *without approximation*. Note that all PSS, PWG, SW and RM kernels are positive definite.

	PSS Kernel	PWG Kernel	SW Kernel	RM Kernel
Time complexity	$O(N^2)$	$O(N^2)$	$O(N^2 \log(N))$	$O(N^2)$
Time complexity with approximation	$O(N)$	$O(N)$	$O(MN \log(N))$	$O(N)$
Metric preservation			✓	✓

Let k_{G_σ} be the Gaussian kernel with a positive parameter σ , and associated reproducing kernel Hilbert space \mathcal{H}_σ . Let $\mu_i := \sum_{p \in \text{Dg}_i} \arctan(C \text{pers}(p)^q) k_{G_\sigma}(\cdot, p) \in \mathcal{H}_\sigma$, where C, q are positive parameter, and for $p = (a, b)$, a persistence of p is that $\text{pers}(p) := b - a$. Let μ_j be defined similarly for Dg_j . Given a parameter $\tau > 0$, the persistence weighted Gaussian kernel is defined as $k_{\text{PWG}}(\text{Dg}_i, \text{Dg}_j) := \exp\left(-\frac{\|\mu_i - \mu_j\|_{\mathcal{H}_\sigma}^2}{2\tau^2}\right)$. The time complexity is $O(N^2)$. Furthermore, (Kusano et al., 2016) also proposed to use the random Fourier features (Rahimi and Recht, 2008) for computing the Gram matrix of m persistent diagrams with $O(mNu + m^2u)$ complexity, where u is the number of random variables using for random Fourier features. Thus, the time complexity can be reduced to be linear in N . (iii) (Carriere et al., 2017) proposed the sliced Wasserstein (SW) kernel, motivated from Wasserstein geometry for PDs. However, it is well-known that the Wasserstein distance is not negative definite. Therefore, it may be necessary to *approximate* the Wasserstein distance to design positive definite kernels on Wasserstein geometry for PDs. Indeed, (Carriere et al., 2017) use the SW distance, which is an approximation of Wasserstein distance, for proposing the positive definite SW kernel, defined as $k_{\text{SW}}(\text{Dg}_i, \text{Dg}_j) := \exp\left(-\frac{d_{\text{SW}}(\text{Dg}_i, \text{Dg}_j)}{2\sigma^2}\right)$. The time complexity for the SW distance $d_{\text{SW}}(\text{Dg}_i, \text{Dg}_j)$ is $O(N^2 \log(N))$, and for its M -projection approximation, it is $O(MN \log(N))$.

For those kernel methods for PDs, only the SW kernel preserves the metric between PDs, that is the Wasserstein geometry. Furthermore, (Carriere et al., 2017) argued that this property should lead to improve the classification power. In this work, we explore an alternative Riemannian manifold geometry for PDs, namely the Fisher information metric which is also known as a particular pull-back metric on Riemannian manifold. Moreover, the proposed positive definite Riemannian manifold kernel is directly built upon the *geodesic* distance of the Fisher information geometry for PDs *without approximation* while it may be necessary to approximate the Wasserstein distance for designing positive definite kernels on Wasserstein geometry for PDs. Addi-

tionally, the time complexity of the Riemannian manifold kernel is also better than the sliced Wasserstein kernel in term of computation. We summary a comparison for the time complexity and metric preservation of those related kernel methods and the proposed Riemannian manifold kernel for PDs in Table 1.

In literature, there is a close related kernel with the Riemannian manifold kernel, namely the diffusion kernel proposed by (Lafferty and Lebanon, 2005). The diffusion kernel is based on the heat equation on the Riemannian manifold defined by the Fisher information metric to exploit the geometric structure of statistical manifolds. Given x, z in the interior of the d -dimension probability simplex, the diffusion kernel is defined as follows,

$$k_{\text{Diff}}(x, z) := (4\pi t)^{-\frac{d-1}{2}} \exp\left(-\frac{1}{t} d_{\mathcal{P}}^2(x, z)\right), \quad (16)$$

where t is a positive parameter. To the best of our knowledge, the diffusion kernel has not been used for measuring the similarity of persistent diagrams. If we use our proposed Riemannian metric (Equation (6)) for persistent diagrams, and then plug the distance into the diffusion kernel, we may get a similar form to our proposed Riemannian manifold kernel. A slight difference is that the diffusion kernel relies on the squared geodesic distance $d_{\mathcal{P}}^2$ while the Riemannian manifold kernel is built upon the geodesic distance $d_{\mathcal{P}}$ itself. However, the Riemannian manifold kernel is positive definite while it is unclear whether the diffusion kernel is positive definite or not⁵.

6. Experimental Results

We evaluated the Riemannian manifold kernel with support vector machines (SVM) on many benchmark datasets. We carried out the persistence scale space (PSS) kernel, the persistence weighted Gaussian (PWG) kernel and the sliced

⁵Although the heat kernel is positive definite, the diffusion kernel on the probability simplex—the heat kernel on multinomial manifold—does not have an explicit form. The k_{Diff} in Equation (16) (Lafferty and Lebanon, 2005) (p. 13) is only its first-order approximation.

Table 2. Results on SVM classification with PSS, PWK, SW and RM kernels for orbit and object shape recognition. The averaged accuracy (%) and standard deviation are shown.

	PSS Kernel	PWG Kernel	SW Kernel	Gaussian Kernel	RM Kernel
Orbit recognition	63.00 ± 3.72	70.40 ± 3.37	78.67 ± 2.71	66.27 ± 2.95	79.20 ± 2.67
Object shape recognition	73.33 ± 4.17	74.83 ± 4.36	76.83 ± 3.75	55.83 ± 5.45	80.00 ± 4.08

Table 3. Averaged accuracy results (%) on SVM classification with PSS, PWK, SW, RM kernels, and with MTF for hemoglobin recognition. The result of MTF with SVM is cited from (Cang et al., 2015).

	MTF	PSS Kernel	PWG Kernel	SW Kernel	Gaussian Kernel	RM Kernel
Accuracy (%)	84.50	83.33	88.89	88.89	83.95	97.53

Wasserstein (SW) kernel as baseline kernels. Additionally, we also consider a Gaussian kernel for the smoothed and normalized measures. It is note that Euclidean metric is not a suitable geometry for the probability simplex (Le and Cuturi, 2015). So, the Gaussian kernel for the smoothed and normalized measures may not work well for PDs. For hyper-parameters, we typically choose them through cross validation. For baseline kernels, we follow their corresponding authors to form sets of hyper-parameter candidates, and the bandwidth of the Gaussian kernel is chosen from $10^{\{-3:1:3\}}$. For the Riemannian manifold kernel, there are 2 hyper-parameters: t (Equation (8)) and σ for smoothing measures (Equation (5)). We choose $1/t$ from $\{q_1, q_2, q_5, q_{10}, q_{20}, q_{50}\}$ where q_s is the $s\%$ of a subset of Riemannian metric between PDs, observed on the training set, and σ from $\{10^{-3:1:3}\}$. For SVM, we use Libsvm (one-vs-one) (Chang and Lin, 2011) for multi-class classification, and choose a regularization parameter of SVM from $\{10^{-2:1:2}\}$. For PDs, we used DIPHA toolbox⁶ to extract 1-dimension topology features with Vietoris-Rips complex filtration.

6.1. Orbit Recognition

It is a synthesized dataset proposed by (Adams et al., 2017) (§6.4.1) for *linked twist map* which is a discrete dynamical system modeling flow. The linked twist map is used to model flows in DNA microarrays (Hertzsch et al., 2007). Given a parameter $r > 0$, and initial positions $(s_0, t_0) \in [0, 1]^2$, its orbit is described as $s_{i+1} = s_i + rt_i(1 - t_i) \bmod 1$, and $t_{i+1} = t_i + rs_{i+1}(1 - s_{i+1}) \bmod 1$. (Adams et al., 2017) proposed 5 classes, corresponding to 5 different parameters $r = 2.5, 3.5, 4, 4.1, 4.3$. For each parameter r , we generated 100 orbits with 1000 points with random initial positions. We randomly split 70%/30% for training and test, and repeated 100 times. The accuracy results on SVM are summarized in the second row in Table 2. The Riemannian manifold kernel performs comparatively with the SW kernel, and outperforms other baseline kernels. Plus, Gaussian kernel does not performance well as expected.

⁶<https://github.com/DIPHA/dipha>

6.2. Object Shape Classification

We consider a 10-class subset⁷ of MPEG7 object shape dataset (Latecki et al., 2000). Each class has 20 samples. We resize each image such that its length is shorter or equal 256, and extract a boundary for object shapes before computing PDs. We also randomly split 70%/30% for training and test, and repeated 100 times. The accuracy results on SVM are summarized in the third row in Table 2. The Riemannian manifold kernel improves performances of other baseline kernels. In addition, Gaussian kernel performances the worst.

6.3. Hemoglobin Classification

We evaluated the Riemannian manifold kernel on Hemoglobin classification for the *taut* and *relaxed* forms (Cang et al., 2015). For each form, there are 9 data points, collected by the X-ray crystallography. As in (Kusano et al., to appear in 2018), we selected 1 data point from each class for test and used the rest for training. Totally, there are 81 runs. We also compared with the molecular topological fingerprint (MTF) for SVM (Cang et al., 2015). We summarize averaged accuracy results on SVM in Table 3. The Riemannian manifold kernel again outperforms other baseline kernels, and also SVM with MTF.

7. Conclusions

In this work, we propose the positive definite Riemannian manifold kernel for persistence diagrams (PDs). The proposed kernel is directly built upon the geodesic distance to preserve the Riemannian manifold geometry for PDs. Moreover, the proposed kernel has many nice properties from both theoretical and practical aspects such as stability, infinite divisibility, comparative time complexity with other kernels on PDs, and improving performances of other baseline kernels in many different tasks on various benchmark datasets.

⁷The 10-classes are: apple, bell, bottle, car, classic, cup, device0, face, Heart and key.

References

Henry Adams, Tegan Emerson, Michael Kirby, Rachel Neville, Chris Peterson, Patrick Shipman, Sofya Chepushtanova, Eric Hanson, Francis Motta, and Lori Ziegelmeier. Persistence images: A stable vector representation of persistent homology. *The Journal of Machine Learning Research*, 18(1):218–252, 2017.

Shun-ichi Amari and Hiroshi Nagaoka. *Methods of information geometry*, volume 191. American Mathematical Soc., 2007.

Peter L Bartlett, Olivier Bousquet, Shahar Mendelson, et al. Local rademacher complexities. *The Annals of Statistics*, 33(4):1497–1537, 2005.

Christian Berg, Jens Peter Reus Christensen, and Paul Ressel. *Harmonic analysis on semigroups*. Springer-Verlag, 1984.

Peter Bubenik. Statistical topological data analysis using persistence landscapes. *The Journal of Machine Learning Research*, 16(1):77–102, 2015.

Zixuan Cang, Lin Mu, Kedi Wu, Kristopher Opron, Kelin Xia, and Guo-Wei Wei. A topological approach for protein classification. *Molecular Based Mathematical Biology*, 3(1), 2015.

Gunnar Carlsson, Tigran Ishkhanov, Vin De Silva, and Afra Zomorodian. On the local behavior of spaces of natural images. *International journal of computer vision*, 76(1):1–12, 2008.

Mathieu Carriere, Marco Cuturi, and Steve Oudot. Sliced Wasserstein kernel for persistence diagrams. In *Proceedings of the 34th International Conference on Machine Learning*, volume 70 of *Proceedings of Machine Learning Research*, pages 664–673, 2017.

Chih-Chung Chang and Chih-Jen Lin. Libsvm: a library for support vector machines. *ACM transactions on intelligent systems and technology (TIST)*, 2(3):27, 2011.

Frederic Chazal and Bertrand Michel. An introduction to topological data analysis: fundamental and practical aspects for data scientists. *arXiv preprint arXiv:1710.04019*, 2017.

Frederic Chazal, Brittany Fasy, Fabrizio Lecci, Bertrand Michel, Alessandro Rinaldo, and Larry Wasserman. Sub-sampling methods for persistent homology. In *International Conference on Machine Learning*, pages 2143–2151, 2015.

Chao Chen and Novi Quadrianto. Clustering high dimensional categorical data via topographical features. In *International Conference on Machine Learning*, pages 2732–2740, 2016.

David Cohen-Steiner, Herbert Edelsbrunner, and John Harer. Stability of persistence diagrams. *Discrete & Computational Geometry*, 37(1):103–120, 2007.

Vin De Silva, Robert Ghrist, et al. Coverage in sensor networks via persistent homology. *Algebraic & Geometric Topology*, 7(1):339–358, 2007.

Herbert Edelsbrunner, David Letscher, and Afra Zomorodian. Topological persistence and simplification. In *Proceedings 41st Annual Symposium on Foundations of Computer Science*, pages 454–463, 2000.

Leslie Greengard and John Strain. The fast gauss transform. *SIAM Journal on Scientific and Statistical Computing*, 12(1):79–94, 1991.

Ying Guo, Peter L Bartlett, John Shawe-Taylor, and Robert C Williamson. Covering numbers for support vector machines. In *Proceedings of the twelfth annual conference on Computational learning theory*, pages 267–277, 1999.

Allen Hatcher. *Algebraic topology*. Cambridge University Press, 2002.

Jan-Martin Hertzsch, Rob Sturman, and Stephen Wiggins. Dna microarrays: design principles for maximizing ergodic mixing. *Small*, 3(2):202–218, 2007.

Christoph Hofer, Roland Kwitt, Marc Niethammer, and Andreas Uhl. Deep learning with topological signatures. In *Advances in Neural Information Processing Systems*, pages 1633–1643, 2017.

Peter M Kasson, Afra Zomorodian, Sanghyun Park, Nina Singhal, Leonidas J Guibas, and Vijay S Pande. Persistent voids: a new structural metric for membrane fusion. *Bioinformatics*, 23(14):1753–1759, 2007.

Soheil Kolouri, Yang Zou, and Gustavo K Rohde. Sliced wasserstein kernels for probability distributions. In *Proceedings of the IEEE Conference on Computer Vision and Pattern Recognition (CVPR)*, pages 5258–5267, 2016.

Genki Kusano, Yasuaki Hiraoka, and Kenji Fukumizu. Persistence weighted gaussian kernel for topological data analysis. In *International Conference on Machine Learning*, pages 2004–2013, 2016.

Genki Kusano, Kenji Fukumizu, and Yasuaki Hiraoka. Kernel method for persistence diagrams via kernel embedding and weight factor. *Journal of Machine Learning Research*, to appear in 2018.

Roland Kwitt, Stefan Huber, Marc Niethammer, Weili Lin, and Ulrich Bauer. Statistical topological data analysis-a kernel perspective. In *Advances in neural information processing systems*, pages 3070–3078, 2015.

John Lafferty and Guy Lebanon. Diffusion kernels on statistical manifolds. *Journal of Machine Learning Research*, 6(Jan):129–163, 2005.

Longin Jan Latecki, Rolf Lakamper, and T Eckhardt. Shape descriptors for non-rigid shapes with a single closed contour. In *Proceedings of the IEEE Conference on Computer Vision and Pattern Recognition (CVPR)*, volume 1, pages 424–429, 2000.

Tam Le and Marco Cuturi. Unsupervised riemannian metric learning for histograms using aitchison transformations. In *International Conference on Machine Learning*, pages 2002–2011, 2015.

Hyekyoung Lee, Moo K Chung, Hyejin Kang, Bung-Nyun Kim, and Dong Soo Lee. Discriminative persistent homology of brain networks. In *International Symposium on Biomedical Imaging: From Nano to Macro*, pages 841–844, 2011.

John M Lee. *Riemannian manifolds: an introduction to curvature*, volume 176. Springer Science & Business Media, 2006.

Shahar Mendelson. On the performance of kernel classes. *Journal of Machine Learning Research*, 4(Oct):759–771, 2003.

Ha Quang Minh, Partha Niyogi, and Yuan Yao. Mercer’s theorem, feature maps, and smoothing. In *International Conference on Computational Learning Theory*, pages 154–168. Springer, 2006.

Vlad I Morariu, Balaji V Srinivasan, Vikas C Raykar, Rama Duraiswami, and Larry S Davis. Automatic online tuning for fast gaussian summation. In *Advances in neural information processing systems*, pages 1113–1120, 2009.

Claus Müller. *Analysis of spherical symmetries in Euclidean spaces*, volume 129. Springer Science & Business Media, 2012.

Ofir Pele and Michael Werman. Fast and robust earth mover’s distances. In *International Conference on Computer Vision*, pages 460–467. IEEE, 2009.

Giovanni Petri, Paul Expert, Federico Turkheimer, Robin Carhart-Harris, David Nutt, Peter J Hellyer, and Francesco Vaccarino. Homological scaffolds of brain functional networks. *Journal of The Royal Society Interface*, 11(101), 2014.

Gabriel Peyre and Marco Cuturi. *Computational Optimal Transport*. 2017. URL <http://optimaltransport.github.io>.

Ali Rahimi and Benjamin Recht. Random features for large-scale kernel machines. In *Advances in neural information processing systems*, pages 1177–1184, 2008.

Jan Reininghaus, Stefan Huber, Ulrich Bauer, and Roland Kwitt. A stable multi-scale kernel for topological machine learning. In *Proceedings of the IEEE conference on computer vision and pattern recognition (CVPR)*, pages 4741–4748, 2015.

I. J. Schoenberg. Positive definite functions on spheres. *Duke Mathematical Journal*, 9:96–108, 1942.

Shai Shalev-Shwartz and Shai Ben-David. *Understanding machine learning: From theory to algorithms*. Cambridge university press, 2014.

Gurjeet Singh, Facundo Memoli, Tigran Ishkhanov, Guillermo Sapiro, Gunnar Carlsson, and Dario L Ringach. Topological analysis of population activity in visual cortex. *Journal of vision*, 8(8):11–11, 2008.

Alex J Smola, Zoltan L Ovari, and Robert C Williamson. Regularization with dot-product kernels. In *Advances in neural information processing systems*, pages 308–314, 2001.

Cédric Villani. *Topics in optimal transportation*. Number 58. American Mathematical Soc., 2003.

Kelin Xia and Guo-Wei Wei. Persistent homology analysis of protein structure, flexibility, and folding. *International journal for numerical methods in biomedical engineering*, 30(8):814–844, 2014.